Nuclear Instruments and Methods in Physics Research A 762 (2014) 135–141

Contents lists available at ScienceDirect

Nuclear Instruments and Methods in Physics Research A

journal homepage: www.elsevier.com/locate/nima

Improving the performance of stainless-steel DC high voltage photoelectron gun cathode electrodes via gas conditioning with helium or krypton

M. BastaniNejad [a,*], A.A. Elmustafa [a], E. Forman [b], J. Clark [b], S. Covert [b], J. Grames [b], J. Hansknecht [b], C. Hernandez-Garcia [b], M. Poelker [b], R. Suleiman [b]

[a] Old Dominion University, Norfolk, VA 23529, USA
[b] Thomas Jefferson National Accelerator Facility, Newport News, VA 23606, USA

ARTICLE INFO

Article history:
Received 6 January 2014
Received in revised form
1 May 2014
Accepted 26 May 2014
Available online 7 June 2014

Keywords:
Field emission
Gas conditioning
Photo electron guns

ABSTRACT

Gas conditioning was shown to eliminate field emission from cathode electrodes used inside DC high voltage photoelectron guns, thus providing a reliable means to operate photoguns at higher voltages and field strengths. Measurements and simulation results indicate that gas conditioning eliminates field emission from cathode electrodes via two mechanisms: sputtering and implantation, with the benefits of implantation reversed by heating the electrode. We have studied five stainless steel electrodes (304L and 316LN) that were polished to approximately 20 nm surface roughness using diamond grit, and evaluated inside a high voltage apparatus to determine the onset of field emission as a function of voltage and field strength. The field emission characteristics of each electrode varied significantly upon the initial application of voltage but improved to nearly the same level after gas conditioning using either helium or krypton, exhibiting less than 10 pA field emission at −225 kV bias voltage with a 50 mm cathode/anode gap, corresponding to a field strength of ~13 MV/m. Field emission could be reduced with either gas, but there were conditions related to gas choice, voltage and field strength that were more favorable than others.

Published by Elsevier B.V.

1. Introduction

Field emission is the primary mechanism that limits the maximum achievable bias voltage, and therefore the electron beam energy, of DC high voltage photoemission electron guns [1–3]. Low level field emission from the cathode electrode has the effect of degrading the vacuum which in turn reduces the photocathode lifetime due to ion bombardment [4–7]. High levels of field emission can damage photogun components, in particular the high voltage insulator.

Many accelerator applications require photoguns operating at ~500 kV bias voltage for producing low emittance beams, comprised of a train of electron bunches [8,9]. The beam emittance degrades in the first few centimeters of acceleration due to space charge forces within the electron bunch. However, space charge forces decrease with the beam energy, hence the desire to operate photoguns at the maximum possible voltage. Unfortunately and without exception, efforts to operate photoguns at 500 kV and maximum field strength greater than 10 MV/m have met with problems due to field emission. Most publications reference beam production at bias voltage less than 400 kV [10–14]. A recent publication [15] describes successful beam delivery at 500 kV using segmented insulators which shield the insulator from harmful field emission.

Groups working on energy recovery linac projects have been at the forefront of efforts to construct very high voltage photoguns. The photoguns at Jefferson Laboratory's Free Electron Laser [16,17] and Daresbury Energy Recovery Linac Prototype [18,19] use stainless steel electrodes polished to mirror-like finish using diamond grit. The Cornell University group uses electropolished stainless steel electrodes [20,21] and groups in Japan rely on chemically-polished titanium alloy electrodes [22]. The cathode/anode gaps in these photoguns are typically ~100 mm with the intention of keeping field strength below 10 MV/m, although higher field strengths are sometimes reached at photogun locations associated with the cathode electrode support structure.

Field emission has been studied for decades, originally as a desirable mechanism to obtain free electron beams. In the 1950s effort was devoted to suppressing and eliminating field emission. Unwanted sources of field emission are assumed to originate primarily from sharp tips protruding from the electrode surface and from inadvertent contamination. Current conditioning [23] is typically the default technique for "processing" a new electrode inside a DC high voltage photogun, whereby voltage is applied to

* Corresponding author.
E-mail address: mahzad@jlab.org (M. BastaniNejad).

http://dx.doi.org/10.1016/j.nima.2014.05.114
0168-9002/Published by Elsevier B.V.

the electrode in small increments, allowing the pre-breakdown field emission current to stabilize and ideally, the field emission current decreases to a smaller level over time as field emission sources "burn off". Current conditioning as a means to eliminate field emission can be unreliable and time consuming.

Gas conditioning as a means to reduce field emission current was originally introduced by Lyman et al., in 1966 [24–26] and used by Bekuma [26,27]. Later, Alpert et al. [25] showed that gas ions selectively bombard metallic micro-protrusions at a higher rate, based on the site's localized field enhancement factor, β. For a time, the effectiveness of gas conditioning was assumed to be related to the transformation of sharp tips into blunt tips, by the process of sputtering. But when gas conditioning was also demonstrated to eliminate field emission from non-metallic emitters [28–30], a full appreciation of the technique grew to include ion implantation which serves to increase the work function of the metal. Latham described the reduction of field emission via implantation as "current quenching" and presented experimental evidence that current quenching was electronic in origin [31,32]. He studied a variety of gasses (H_2, D_2, He, Ar, N_2, SF_6) and demonstrated that each was effective at eliminating field emission but the voltage at which the process was performed was a critical parameter, indicating that helium was more effective at eliminating field emission at lower voltage while heavier gasses were more effective at higher voltage [33].

In the 1970s when the DC high voltage photogun community worked vigorously to construct spin-polarized electron sources using GaAs photocathodes, there were many instances of problematic field emission, even for photoguns operating at just 100 kV. Frequently, the field emission was attributed to inadvertent deposition of cesium on the cathode electrode (with the cesium originating from the photocathode activation process). Load-locked photogun designs helped to solve this problem, by moving the photocathode activation process outside the high voltage chamber. Field emission problems that remained were often "solved" by operating the photogun at a reduced voltage. Only relatively recently [12], with the increased interest in low-emittance beams and very high bias voltages, has the photogun community sought alternatives to the current conditioning technique.

In this work, stainless steel (304L and 316LN) electrodes were evaluated inside an ultrahigh vacuum apparatus at voltages to −225 kV with cathode/anode gaps ranging from 20 to 50 mm, providing a maximum field strength of ~18 MV/m for the smallest gap. All of the stainless steel electrodes were polished to mirror-like finish with root-mean-square surface roughness between 10 and 30 nm [36] using silicon carbide paper and successively finer diamond grit. Field emission results among the samples varied significantly upon initial application of voltage. This variability is likely attributable to inadvertent contamination of the electrode surface.

Each electrode was then gas conditioned consecutively with helium or krypton: if field emission persisted following conditioning with one gas species, further conditioning was implemented using the other gas. Conditions were varied to investigate whether one gas was more effective than the other, and to determine under what conditions field emission was most efficiently reduced. Ultimately, both gasses demonstrated success at eliminating field emission, however it was difficult to make firm conclusions as to which gas worked best, because once field emission was eliminated using one gas, further gas conditioning with the other gas was not possible.

The performance of all electrodes improved to comparable levels with inert gas conditioning, exhibiting field emission less than 10 pA at −225 kV bias voltage with a 50 mm cathode/anode gap, corresponding to a field strength of ~13 MV/m. The benefit of inert gas conditioning was partially eliminated by purposely heating the electrode to temperature ~250 °C for hours, confirming empirical observations reported in Ref. [14] Experimental results and accompanying modeling using the programs SRIM and TRIM (Stopping Range of Ions in Matter, and Transport of Ions in Matter, respectively) [37] suggest that gas conditioning serves to eliminate field emission via sputtering but also via ion implantation which would serve to increase the work function near the surface of the electrode.

2. Helium and krypton gas conditioning

Literature data [34,35] on electron impact ionization was used to calculate the electron impact ionization probabilities (cross section) for helium and krypton as a function of electron beam energy (Fig. 1a). The two curves mimic each other, however with the ionization probability of krypton roughly an order of magnitude higher than helium. The peak ionization for both gas species occurs at ~100 V, and drops by more than three orders of magnitude at 225 kV, the maximum voltage studied in this work. It is important to note that the energy spectrum of the field emitted electrons within the cathode/anode gap is broad, with electrons leaving the cathode electrode at zero velocity, and then gaining energy until reaching the anode. Ionization probabilities can be used to estimate the ion production rate over a small distance, dx, by considering the following equation,

$$\text{Number of ions } (s^{-1}) = n_g n_e CS(T)dx \quad (1)$$

where n_g describes the gas atomic number density (atoms/m^3) introduced into the vacuum chamber, n_e is the number of electrons per second within the cathode/anode gap arising from field emission, and CS represents the ionization cross section illustrated in Fig. 1a. The symbol T represents the kinetic energy of the emitted electron at a distance x from the cathode surface, equal to $(x/Gap)eV$ where Gap describes the distance between the

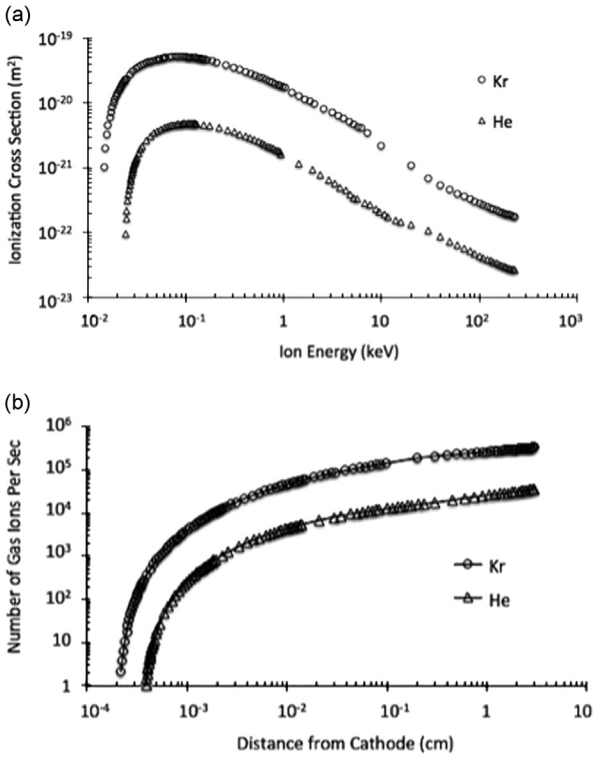

Fig. 1. (a) Ionization cross section for helium and krypton, and (b) calculated ion yield per second as a function of distance from the cathode surface assuming a pressure of 5×10^{-6} Torr and field emission current of 13 nA at 200 kV.

cathode and anode electrodes, e is the charge of the electron and V is the bias voltage applied to the cathode electrode. To determine the total number of ions reaching the cathode surface per second as a function of distance from cathode surface, Eq. (1) can be integrated with respect to kinetic energy and by noting that $dx = Gap/\mathrm{eV}\, dT$,

$$\text{Total Number of ions } (\mathrm{s}^{-1}) = n_g n_e \frac{Gap}{\mathrm{eV}} \int_0^{(x/Gap)\mathrm{eV}} CS(T)dT \qquad (2)$$

The following parameters where used to obtain the result in Fig. 1b: gas pressure 5×10^{-6} Torr, a field emission current of 13 nA at the cathode bias voltage of 200 kV, with the cathode/anode gap set to 3 cm. Notice that nearly half of all ions originate within 1 mm of the cathode electrode surface.

From a sputtering point of view, massive krypton will be more effective at turning sharp field emitter tips into blunt tips compared to helium, but other factors must be considered when implementing gas conditioning inside a DC high voltage photogun, including the cathode/anode geometry, the orientation of electrostatic field lines, and where the ions are created within the cathode/anode gap. Most DC high voltage photoguns employ curved electrodes, which in turn, produce curved electric field lines. Electrons will follow these curved electric field lines but comparatively slow moving ions will have trajectories that can deviate significantly. Only ions produced at locations with straight electric field lines, or near the cathode surface are guaranteed to impact the electrode near the field emitter. In summary, the location where the ion was created within the cathode/anode gap determines the energy of the ion at impact, which in turn influences sputtering yield and implantation depth. The curved field lines will reduce the likelihood of higher-energy ions produced near the anode reaching the field emitter.

3. Experiment

3.1. Apparatus

Pierce-type cathodes with 25° focusing angle (6.35 cm dia., 2.85 cm thick) were attached to an inverted insulator that extends into the ultrahigh vacuum test chamber (Fig. 2). Each electrode had a shape identical to electrodes used at the Continuous Electron Beam Accelerator Facility (CEBAF) [38] with a hole in the middle (1.28 cm dia.) to accommodate a GaAs photocathode if it were used in an actual polarized photogun. However for these tests, a piece of polished stainless steel was used in place of the GaAs photocathode. The electrodes were polished with silicon carbide paper and diamond paste of successively finer grit as described in Ref. [39].

The polished stainless steel anode was a flat plate with a Rogowski edge profile, electrically isolated from ground and attached to a sensitive current meter (Keithley electrometer model 617). The anode could be moved up or down to vary the cathode/anode gap and therefore the field strength. Cathode/anode gaps discussed in this paper refer to the distance between the curved portion of the cathode closest to the anode surface. Field emission was assumed to originate from the region of the cathode electrode subjected to the highest field strength, which corresponds to an annular region with radius slightly larger than the portion of the electrode closest to the anode [39].

A −225 kV commercial high voltage power supply was used for the experiment. The high voltage power supply and the ceramic insulator accommodate “industry standard” high voltage cables with R-28 connectors. A 100 MΩ conditioning resistor was placed in series with the cathode electrode via an oil tank that served to protect the apparatus in case of sudden discharge of stored energy. The resistor also serves to protect the electrode via a negative feedback mechanism – as current increases, a larger voltage drop occurs across the resistor, reducing voltage at the electrode.

Prior to the application of high voltage, the entire vacuum apparatus was baked at 200 °C for 30 h to achieve vacuum level in the 5×10^{-11} Torr range. Pumping was provided by a 220 L/s ion pump and a SAES Getters GP-500 non-evaporable getter pump which was partially activated during the bakeout. Every effort was made to keep the vacuum conditions consistent from sample-to-sample.

An assessment of the field emission properties of each test electrode involved monitoring vacuum level via the ion pump current, x-ray radiation with Geiger monitors placed around the apparatus, and the anode current with a digital electro-meter, while increasing the applied voltage. High voltage was first applied to the electrode using the largest cathode/anode gap of 50 mm where the maximum field strength reaches 13 MV/m at −225 kV bias. Upon successful high voltage processing (aka, current conditioning), the gap could be decreased to achieve higher field strength. The smallest gap used for the tests was 20 mm and provided maximum field strength of ∼18 MV/m when the cathode was biased at −225 kV. Field strength values were estimated using the electrostatic field mapping program POISSON [40]. Smaller gaps provided significantly higher field strength, but sometimes produced catastrophic breakdown and electrode damage.

3.2. Gas conditioning protocol

Gas conditioning involved introducing an inert gas into the vacuum chamber while the cathode electrode was biased at high voltage using a gap/field strength that produced significant field

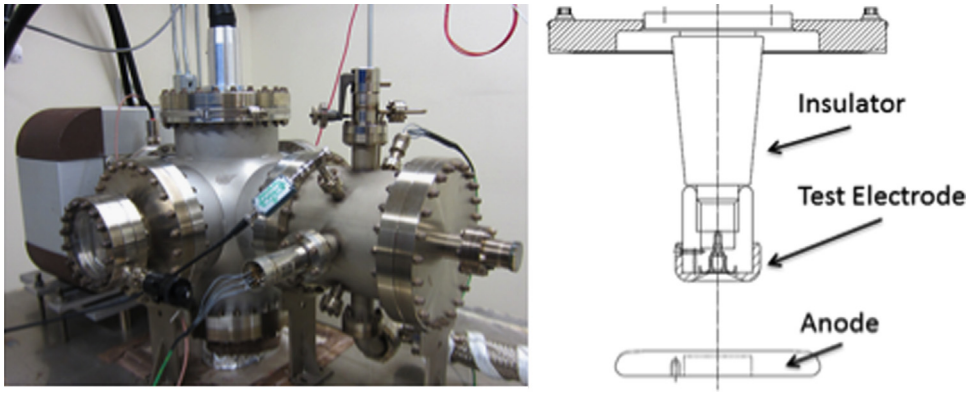

Fig. 2. Photograph of the dc high voltage field emission test stand used to evaluate each cathode electrode (left), a schematic view of the insulator, test electrode and anode used to collect the field emission (right).

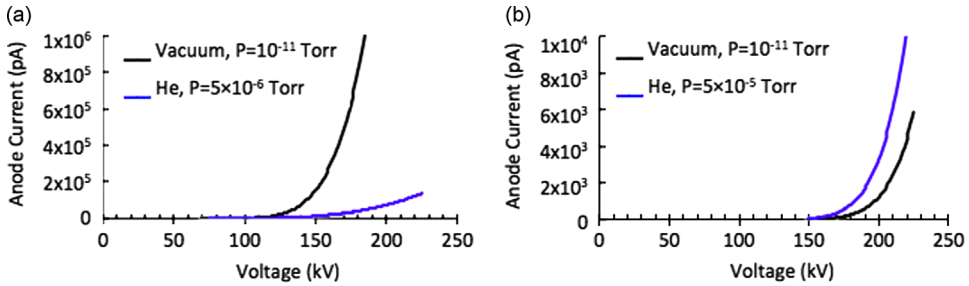

Fig. 3. Examples of (a) current quenching using a10 mm cathode/anode gap, and (b) current amplification using a 30 mm cathode/anode gap, during helium gas conditioning at different pressures.

emission ($\sim$ few μAs or lower). Gas was introduced to the vacuum apparatus via a leak valve set to provide pressure in the range of $\sim 5\times 10^{-6}$ to $\sim 5\times 10^{-4}$ Torr (nitrogen equivalent). A sudden reduction in anode current was indicative of the elimination of a field emission site. Gas conditioning typically was performed for 30–60 min and repeated multiple times, depending on the performance of the test electrode in the field emission reduction process. Details relating to implementation can be found in Ref. [39].

Inert gas pressure and cathode/anode gap could be varied to observe two distinct anode current trends: current amplification and current quenching. Current amplification can be explained by noting that the ionization of the supplied gas produces additional free electrons that travel to the anode in addition to those originating from field emission sites. Furthermore, ions bombarding the cathode electrode, and electrons striking the anode electrode desorb additional gas (most likely surface-bound hydrogen) that can in turn become ionized. The other trend – current quenching – describes the situation where the observed anode current is reduced during gas conditioning. This phenomenon occurs when a sufficient number of ions blanket the electrode surface, increasing the work function of the material, thereby quenching the field emission (at least temporarily, during gas conditioning).

Fig. 3 shows examples of both anode-current trends observed using the same electrode but under different conditions: helium pressure 5×10^{-5} Torr versus 5×10^{-6} Torr, and cathode anode gap 10 and 30 mm. The black (blue) lines represent the observed anode current before (during) gas conditioning, as a function of applied high voltage. Field emission could be reduced under both conditions. These tests did not reveal that inert gas pressure, or the magnitude of the anode current, were key factors in determining the efficacy of gas conditioning.

4. Results

4.1. Field emission versus voltage (I–V curves)

The field emission characteristics of four diamond-paste polished stainless steel electrodes are presented in Fig. 4. Each plot shows field emission current as a function of voltage at four different cathode–anode gaps, before and after gas conditioning. During the initial application of voltage, the 304L electrodes exhibited field emission at bias voltage at or below -100 kV, whereas the 316LN electrode performed better, with field emission onset of ~ -150 kV or higher. It should be noted that the small sample set precludes making a definitive statement about properties of specific grades of steel. After gas conditioning, all four electrodes exhibited similar performance, with no field emission (<10 pA) at 50 mm gap and -225 kV bias voltage corresponding to a field strength of 13 MV/m. One electrode required just one gas conditioning cycle, while the other electrodes required multiple cycles. For those electrodes that required extended conditioning, implementation was alternated between gas species in 30–60 min intervals until no noticeable improvement was observed. The longest cumulative conditioning period was $\sim$3.5 h.

Table 1 lists the field strength (at the highest-field strength region of the cathode) at which each electrode produced 100 pA of field emission. The value 100 pA was chosen because it was large enough to accurately apply a Fowler–Nordheim fit to the data. Before gas conditioning most of the electrodes exhibited field emission at field strengths between 5 and 10 MV/m. After gas conditioning, for the gaps 40 and 50 mm, none of the electrodes exhibited 100 pA of field emission corresponding to field strengths 13.8 and 12.6 MV/m, respectively.

It is common to re-plot *I–V* curves like those in Fig. 4 as Fowler–Nordheim line plots, showing the variation of the quantity $\log(I/E^2)$ as a function of $1/E$, where I is the field emission current and E is the average surface field strength. Such a representation can be used to estimate the field enhancement factor, β, and the field emission emitter area, A_e, using the expressions below [39]:

$$\text{slope} = \frac{d(\log_{10} I/E^2)}{d(1/E)} = -\frac{2.84\times 10^9 \varphi^{1.5}}{\beta} \tag{3}$$

$$\text{intercept} = \text{Log}_{10}(I_F/E^2)_{E\to\infty} = \text{Log}_{10}\left[\frac{1.54\times 10^{-6} A_e \beta^2 \times 10^{4.52\varphi^{-0.5}}}{\varphi}\right] \tag{4}$$

where φ is the work function of the material. As illustrated in Table 2, gas conditioning yielded smaller field enhancement factors and larger emitter areas for each electrode, consistent with the notion that field emitter tips become blunted and wider as a result of gas conditioning. Considering all electrodes, the average value for the field enhancement factor, β, reduced from 473 to 197, and the calculated emitting area increased from an average value of 4.5×10^{-18} to 2.8×10^{-17} m^2. Also noteworthy, the individual post-gas conditioning values for β and A_e exhibit smaller deviations from the average values, suggesting that gas conditioning provides a means to evaluate the true field emission characteristics of materials, rather than the unpredictable properties of an electrode suffering contamination. However, it should be mentioned that field emission from large area electrodes likely originates from multiple emitters, whereas Eqs. (3) and (4) were derived for a single emitter. Some researchers question the validity of the Fowler–Nordheim line plot analysis for large area electrodes, wondering if calculated values of β and A_e represent characteristics of one emitter or a "distribution" of values associated with many emitters [41].

4.2. Helium versus krypton

Effort was devoted to determining the relative effectiveness of helium versus krypton. Electrodes were conditioned with one gas under different pressure and gap conditions, and then conditioned using the other gas if field emission persisted. However, the

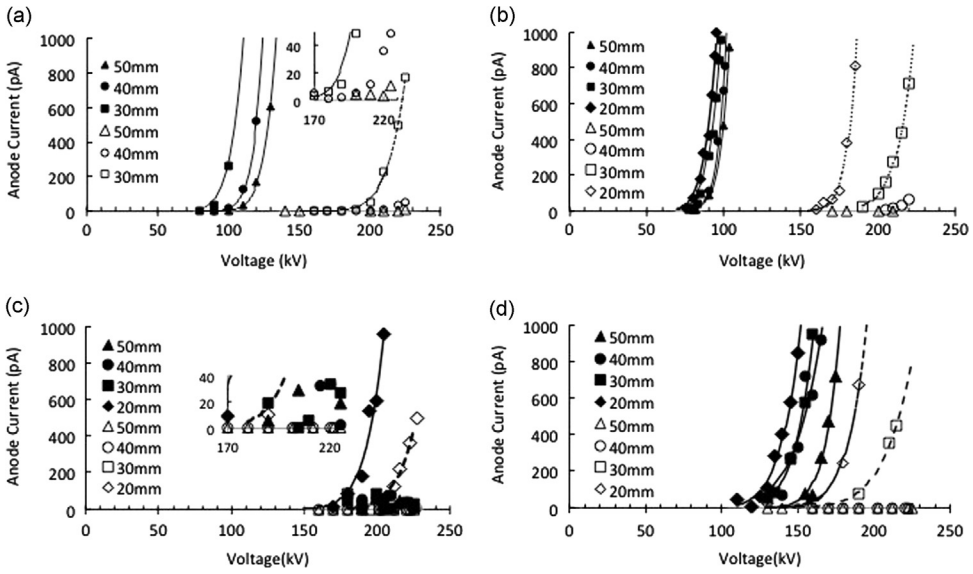

Fig. 4. Field emission current versus bias voltage and anode/cathode gap for 304L stainless steel electrodes (top) and 316LN electrodes (bottom). Each plot shows field emission behavior before (solid symbols) and after (open symbols) gas conditioning with helium and krypton. For all cases the lines between data points represent Fowler–Nordheim fits. The error in these measurements is comparable to the size of the data point symbol, and smaller for electrodes post-gas conditioning.

Table 1
The field strength (MV/m) at which each electrode exhibited 100 pA of field emission at different gaps before and after gas conditioning. For entries with (>) symbol, field emission current did not exceed 100 pA at −225 kV, and consequently, the field strength must exceed the maximum value provided by the high voltage power supply. The labels "1" and "2" are bookkeeping designations that denote different electrodes of the same material.

Turn on field strength (MV/m) at 100 pA, before gas processing vs. gaps				
Gap (mm)	**304L#1**	**304L#2**	**316LN#1**	**316LN#2**
50	6.4	4.9	> 12.6	8.7
40	6.6	5.4	> 13.8	8.1
30	6.2	5.5	> 15	9.1
20		6.6	15	10.5
Turn on field strength (MV/m) at 100 pA, after gas processing vs. gaps				
50	> 12.6	> 12.6	> 12.6	> 12.6
40	> 13.8	> 13.8	> 13.8	> 13.8
30	13.6	13.5	> 15	12.9
20		14.4	17.3	14.1

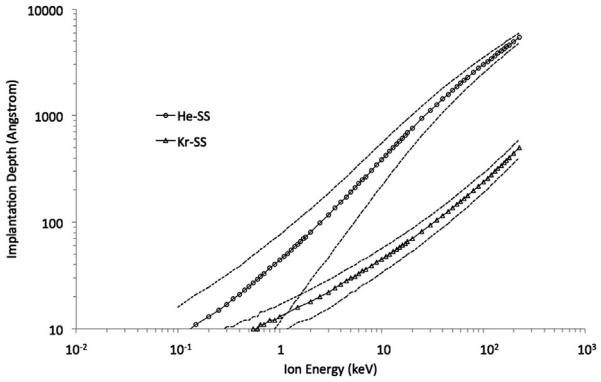

Fig. 5. Helium (top) and krypton (bottom) ion implantation depth for helium and krypton as a function of ion energy. The dashed lines with data points represent the implantation depth corresponding to the peak of the distribution, with adjacent solid lines representing depths ±0.5 sigma from the peak value.

Table 2
Summary of Fowler–Nordheim line plot analysis: field enhancement factor, β, and emitting area, A_e, before and after gas conditioning, for four stainless steel electrodes. The statistical variations in the values listed below are small, with chi-squared fit parameters close to unity. More significant are the large systematic variations between different electrodes, which point to the unpredictable nature of field emission, and challenges associated with preparing identical electrode samples. The labels "1" and "2" are bookkeeping designations that denote different electrodes of the same material.

	304L#1	**304L#2**	**316LN#1**	**316LN#2**
β/pre-gas	228	972	217	475
β/post-gas	134	299	185	171
A_e (m^2)/pre-gas	9.7×10^{-19}	8.4×10^{-20}	1.7×10^{-17}	2.5×10^{-20}
A_e (m^2)/post-gas	1.1×10^{-17}	7.1×10^{-17}	3×10^{-17}	1.4×10^{-19}

performance of the electrode was very difficult to control: once the electrode performance improved to a high level, further gas conditioning was not possible (i.e., the electrode did not field emit and consequently, ions were not created). Smaller gaps could be used to achieve significantly higher field strength, which could initiate more field emission, but often small gaps resulted in breakdown which damaged the electrode. A cumulative assessment based on tests of five electrodes led to the following generalized observation: helium was more effective at eliminating field emission using lower voltage and smaller gaps, whereas krypton was more effective at higher voltage and larger gaps. But it must be stated that this is a very preliminary "conclusion": there were examples of effective field emission reduction under conditions contrary to this statement that could be related to effects of any gas on a virgin electrode regardless of the gas kind. It must also be noted that krypton gas conditioning at small gaps sometimes resulted in degraded performance, serving to enhance field emission.

To better understand the experimental results, the computer simulation codes SRIM and TRIM (Stopping Range of Ions in Matter, and Transport of Ions in Matter) [25] were used to estimate the stopping depth of implanted gas ions within the cathode electrode and the level of sputtering. Fig. 5 shows the implantation depth for monoenergetic helium and krypton ions, as a function of ion energy. Ion implantation depth represents a distribution of values: the dashed line for each gas species shows the implantation depth for the peak of the distribution, with adjacent lines representing the range of depths ±0.5 sigma from the peak. Comparing the two simulations, it is obvious that helium ions

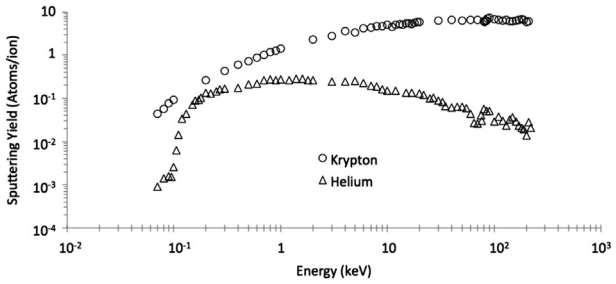

Fig. 6. Sputtering yield of monoenergetic helium and krypton ions on stainless steel, versus ion energy.

penetrate much deeper into the stainless steel compared to krypton. Helium ions are implanted at depths to 6000 Å, whereas krypton ions are implanted at depths <1000 Å. Assuming implanted ions serve to reduce field emission (at least in part) due to increased work function, it would be beneficial to helium gas process at lower voltage, where the implanted ions are closer to the surface. This result is consistent with experimental observation – helium gas processing was generally more effective at lower voltages and smaller cathode/anode gaps. More massive krypton ions are implanted at shallow depths for all ion energies tested. Consequently, krypton ion implantation would serve to increase the work function of the electrode for any ion energy tested.

Fig. 6 shows the results obtained using the program TRIM, which characterizes the sputtering yield of helium and krypton ions on stainless steel, as a function of ion energy. Krypton has a significantly higher sputter yield compared to helium, over the entire ion energy range tested. For krypton ions with energy greater than 1 kV, multiple atoms are sputtered from stainless steel for each bombarding krypton ion, whereas many helium ions are required to sputter away a single atom from stainless steel over the entire energy range tested. This would certainly be beneficial when dealing with an electrode suffering from contamination, and sputtering would serve to transform sharp tips into blunt tips, assuming the ions are delivered to the emitter. But excessive sputtering can lead to enhanced field emission [42] and this could potentially explain why sometimes krypton gas conditioning resulted in higher levels of field emission from test electrodes.

4.3. Reversing the effects of gas conditioning

In order to decouple the benefits of ion implantation and sputtering, a fifth stainless steel electrode was gas conditioned and then heated to 250 °C in situ, for approximately 8 h, using a small heater inserted into the bore of the ceramic insulator. These heating conditions provide ample time for implanted ions to diffuse from the electrode surface and into the bulk electrode material (per Fick's law), because the number of implanted ions is relatively small. The logic behind the heating test was the following. If the field emission suppression mechanism was purely due to sputtering, then heating would not change the field emission current after conditioning. If the mechanism was purely due to changes in the work function, then heating would reverse the field emission current back to levels prior to conditioning. Fig. 7a shows field emission current as a function of voltage for one of the 316LN electrodes at 40 mm gap before (solid black circles) and after (open black circles) gas conditioning, as well as after cathode electrode heating (red). The field emission levels increased after heating, but the electrode still performed better than it did initially, suggesting that the cumulative benefit of gas conditioning is composed of both sputtering and ion implantation, with the latter being reversible. These results indicate that heating the

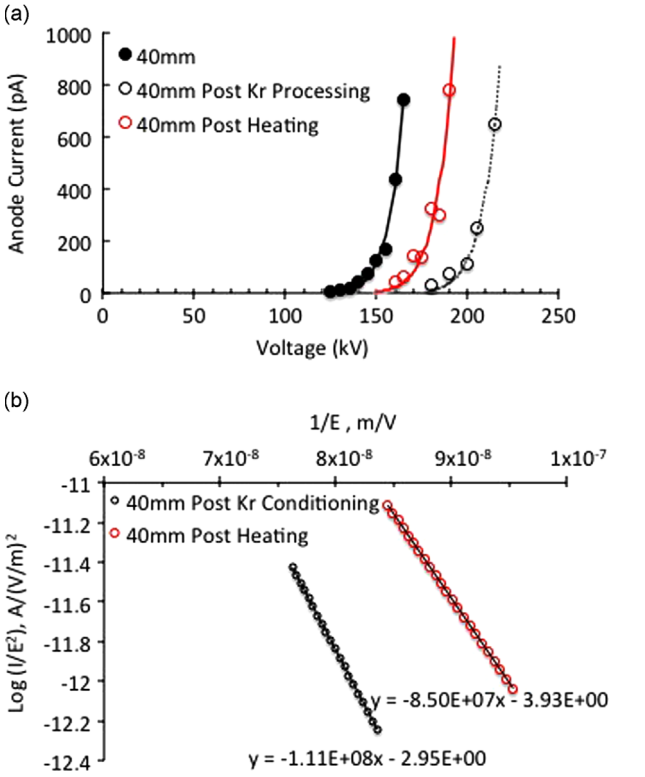

Fig. 7. (a) Field emission current as a function of bias voltage for a 40 mm cathode/anode gap, before (black) and after (open) gas conditioning and after heating (red). (b) Fowler–Nordheim logarithmic line plots of the post-Kr-processing and post-heating results shown above. The change in slope of the two lines was used to estimate the change in the work function associated with ion implantation.

electrode served to enhance diffusion of ions within the material, reducing the concentration of ions at the surface of the electrode.

To estimate the increase in the work function associated with gas conditioning, the *I–V* curves representing the post-Kr-processing and post-heating results were re-plotted as Fowler–Nordheim line plots (Fig. 7b). The field enhancement factor β was calculated from the post-heating result, by evaluating the slope of the line and assuming a typical work function for stainless steel of 4.4 eV. It is reasonable to assume that heating the electrode does not change the physical characteristics of the electrode (i.e., β remains the same). For the calculated value of the field enhancement factor ($\beta=236$), the work function must increase by $\sim$1.16 eV to fit the post-krypton processing result, an amount consistent with reports in literature [43].

5. Conclusion

Five stainless steel electrodes (304L and 316LN) were polished to approximately 20 nm surface roughness using diamond grit and evaluated inside an ultrahigh vacuum test stand to determine the onset of field emission as a function of voltage and field strength. The field emission characteristics of each electrode varied significantly upon the initial application of voltage, with the 316LN stainless steel electrodes performing better than the 304L stainless steel electrodes. The performance of all electrodes improved to nearly the same level using gas conditioning with helium and/or krypton, with field emission less than 10 pA at -225 kV bias voltage and for a 50 mm cathode/anode gap, corresponding to a field strength of $\sim$13 MV/m. Some electrodes reached higher field strengths without field emission, at smaller gaps. Field emission could be reduced using either gas, but helium gas conditioning was more effective at lower voltage

and small gaps (10–20 mm), whereas krypton gas conditioning was more effective at higher voltages and larger gaps (30–50 mm). Both gasses were effective at pressures in the range of $5–50 \times 10^{-6}$ Torr and the benefits of gas conditioning were typically realized during ~20 min-long processing periods.

Measurements and accompanying simulation results obtained using the computer simulation codes SRIM/TRIM suggest that gas conditioning effectively eliminates field emission sites via sputtering but also as a result of ion implantation which serves to increase the work function of the electrode. This statement is supported by the observation that field emission suppression effects of ion implantation could be partially reversed by heating the electrode, which depletes the electrode surface of implanted ions due to desorption and diffusion. The simulation results also support the general trend that helium gas conditioning was more effective at lower voltages because this yields a shallow implantation depth, which is better suited to increasing the work function of the metal. Empirical observations reported in Ref. [14] are now understood with the contributions presented in this work.

There are practical considerations associated with gas conditioning that were not addressed experimentally or using the simulation software, namely, curved electrodes generate curved field lines. For example, krypton offers advantages over helium: it is easier to ionize compared to helium and has a higher sputtering yield, however, depending on location of the field emitter, krypton ions may not follow the field lines to the location of the field emitter. Another issue that was not raised in the paper relates to x-ray radiation – krypton ion bombardment generates significantly higher levels of x-ray radiation which could conceivably be problematic for some users depending on their available shielding.

Future work could employ an ion gun to sputter-clean and implant the entire electrode, rather than just locations near an active field emitter. The ion gun would also provide a monochromatic ion beam that could provide a more accurate experimental assessment of sputter yield and the most effective implant depth, and conditions could be more accurately modeled.

The results and methodologies presented are highly significant to the present development of 500 kV DC photoemission guns at various institutions (Cornell, JLab, JAEA, Daresbury) with the goal to generate ultra-bright electron beams required for proposed Free Electron Lasers based on energy recovery accelerators to produce x-ray beams with unprecedented flux and brilliance.

Acknowledgments

The authors wish to thank Md. Abdullah Mamun and M. Stutzman with assistance in calculating the rate of diffusion of implanted ions from the surface of the electrode, due to intentional electrode heating, and Phillip Williams of NASA Langley, Hampton VA, for help with surface measurements of the electrodes.

Notice: Authored by Jefferson Science Associates under United states DOE Contract no. DE-AC05-84ER40150 and with funding from the DOE Office of High Energy Physics and the Americas Region ILC R&D program. The U.S. Government retains a non-exclusive, paid-up, irrevocable, world-wide license to publish or reproduce this manuscript for U.S. Government purposes.

References

[1] J. Rosenzweig, G. Travish, L. Serafini, The Physics and Applications of High Brightness Electron Beams, World Scientific Publishing Company, Inc. River edge, NJ, USA, 2004.
[2] I.V. Bazarov, B.M. Dunham, C.K. Sinclair, Physical Review Letters 102 (2009) 104801.
[3] C.K..Sinclair, Proceedings of the Particle Accelerator Conference, 76 (2003).
[4] K. Aulenbacher, et al., Nuclear Instruments and Methods in Physics Research A 391 (1997) 498.
[5] H.G. Andresen, et al., Proceedings of Workshop on Photocathodes for Polarized Electron Sources for Accelerators, SLAC (1993).
[6] C.K. Sinclair, Proceedings of the Particle Accelerator Conference, New York, NY, (1999).
[7] E. Pozdeyev, Proceedings of the Particle Accelerator Conference, Albuquerque, New Mexico, USA (2007).
[8] I.V. Bazarov, D.G. Ouzounov, B.M. Dunham, S.A. Belomestnykh, Y. Li, X. Liu, R. E. Meller, J. Sikora, C.K. Sinclair, F.W. Wise, T. Miyajima, Physical Review Special Topics: Accelerator Beam 11 (2008) 040702.
[9] R. Hajima, R. Nagai, Nuclear Instruments and Methods in Physics Research A 557 (2006) 103.
[10] C. Hernandez-Garcia et al., Proceedings of the 45th ICFA Advanced Beam Dynamics Workshop, Cornell University, Ithaca, NY, (2009), pp. 37–39.
[11] L.B. Jones, S.P. Jamison, Y.M. Saveliev, K.J. Middleman, and S.L. Smith, Proceedings of the 18th International Symposium on High Energy Spin Physics, AIP Conference Proceedings 1149 (2008), p. 1084.
[12] B.M. Dunham and K.W. Smolenski, in: Proceedings of IEEE International Power Modulator and High Voltage Conference, Atlanta GA, (2010), pp. 98–101.
[13] N. Nishimori, R. Nagai, H. Iijima, Y. Honda, T. Muto, M. Kuriki, M. Yamamoto, S. Okumi, T. Nakanishi, and R. Hajima, in Proceedings of the 18th International Symposium on High Energy Spin Physics AIP Conf. Proc. 1149, 1094 (2008).
[14] C. Hernandez Garcia, S.V. Benson, G. Biallas, D. Bullard, P. Evtushenko, K. Jordan, M. Klopf, D. Sexton, C. Tennant, R. Walker, and G. Williams, Thomas Jefferson National Accelerator Facility, Newport News, VA 23606, AIP Conference Proceedings 1149, pp. 1071–1076.
[15] Nishimori, et al., Applied Physics Letters 102 (2013) 234103.
[16] C.K. Sinclair, Nuclear Instruments and Methods in Physics Research A 557 (2006) 69.
[17] C. Hernandez-Garcia, et al., in: Proceedings of the 26th International Free Electron Laser Conference, Trieste, Italy, (2004), p. 558.
[18] D.J. Holder, N. Bliss, J.A. Clarke, P.A. McIntosh, M.W. Poole, E.A. Seddon and S.L. Smith, in: Proceedings of EPAC, CCLRC Daresbury Laboratory, U.K., Edinburgh, Scotland, (2006).
[19] Y.M. Saveliev, F. Jackson, J. Jones, J. McKenzie, in: Proceedings of IPAC, STFC Daresbury Laboratory, ASTeC & Cockcroft Institute, UK, New Orleans, Louisiana, USA, (2012).
[20] B.M. Dunham, et al., in: Proceedings of IPAC 2012, New Orleans, Louisiana, (May 2012).
[21] K. Smolenski, I. Bazarov, B. Dunham, H. Li, Y. Li, X. Liu, D. Ouzounov, C. Sinclair, AIP Conference Proceedings 1149 (2008), pp. 1077–1083.
[22] R. Nagai, et al., High-voltage testing of a 500-kV dc photocathode electron gun, Review of Scientific Instruments 81 (2010) 033304.
[23] R.V. Latham, High Voltage Vacuum Insulation, Academic Press, London, 1995.
[24] E.M. Lyman, D.A. Lee, H.E. Tomaschke and D. Alpert, in: Proceedings of II-DEIV, (1966), pp. 33–39.
[25] D. Alpert, D.A. Lee, E.M. Lyman, H.E. Tomasche, Journal of Applied Physics 38 (1967) 880.
[26] G.P. Beukema, Journal of Physics D: Applied Physics 7 (1974) 1740.
[27] G.P. Beukema, Physica C 61 (1972) 259.
[28] C.S. Athwal, R.V. Latham, Physica C 104 (1981) 189–195.
[29] R.V. Latham, Vacuum 32 (1982) 137.
[30] K.H. Bayliss, R.V. Latham, Proceedings of the Royal Society 403 (1986) 285.
[31] S. Bajic, R.V. Latham, IEEE Transactions on Electrical Insulation 23 (1988) 27.
[32] S. Bajic, R.V. Latham, Journal of Physics D: Applied Physics 21 (1988) 943.
[33] S. Bajic, A.M. Abbot, R.V. Latham, IEEE Transactions on Electrical Insulation 24 (6) (1989) 891–896.
[34] M. Reiser, Theory and Design of Charged Particle Beams, John Wiley & Sons, Inc., New York, 1994.
[35] L.J. Kieffer, G.H. Dunn, Reviews of Modern Physics 38 (1) (1966) 1.
[36] B. Bhushan, J.C. Wyant, J. Meiling, Wear 122 (3) (1988) 301.
[37] J. Biersack, J.P. Ziegler, M.D. Ziegler, (1985) ⟨http://www.srim.org⟩.
[38] C.K. Sinclair, P.A. Adderley, B.M. Dunham, J.C. Hansknecht, P. Hartmann, M. Poelker, J.S. Price, P.M. Rutt, W.J. Schneider, M. Steigerwald, Physical Review Special Topics Accelerators and Beams 10 (2007) 023501.
[39] M. BastaniNejad, Md. Abdullah Mohamed, A.A. Elmustafa, P. Adderley, J. Clark, S. Covert, J. Hansknecht, C. Hernandez-Garcia, M. Poelker, R. Mammei, K. Surles-Law, P. Williams, Physical Review Special Topics Accelerators and Beams 15 (2012) 083502.
[40] K. Halbach, Lawrence Livermore National Laboratory Technical Report No. UCRL-17436, (1967).
[41] H. Tomaschke, D. Alpert, Journal of Applied Physics 38 (1967) 881.
[42] Jon Orloff, Handbook of Charged Particle Optics, second ed., CRC Press, Boca raton, FL, USA, 2008 (October 24).
[43] O.Y. Kolesnychenko, O.I. Shklyarevskii, H. van Kempen, Physica B 284 (2000) 1257.